JKAU: Eng. Sci., **vol. 11 No. 2,** pp. 11-40 (1419 A.H. / 1999 A.D.)

Discharge Growth Simulation between Parallel-Plate Electrodes Using Various Computation Techniques

A.H. MUFTI
High Voltage Laboratory, Electrical and Computer Engineering Department,
Faculty of Engineering, King Abdulaziz University,
Jeddah, Saudi Arabia

ABSTRACT. In this work, a simulation of the discharge growth between parallel-plate electrodes is built up based on various computation techniques. The continuity equations of different particle species existing in the discharge are solved by the characteristic method. The electric field is evaluated by a disc method and one dimensional Poisson's equation. Excited atoms or molecules and photons due to photoionization process is also included. The secondary electrons due to u.v. light, positive ion and delayed and/or undelayed photon cathode bombardment are evaluated. In this respect various computation techniques led to select the most accurate method used in the discharge simulation which enables the discharge to be traced to later stages. The total gap current and breakdown time are discussed. N_2 gas is implemented in gap to study the discharge growth using various computation techniques.

1. Introduction

The study of the discharge growth before the occurrence of the breakdown under applying high voltage is a significant subject from the electrical engineering point of view, because such phenomena may occur naturally within the insulation system in the high voltage equipment. Much efforts have been made to study the discharge growth experimentally and theoretically. The theoretical method is preferred since it has low cost and certain assumptions may be considered to simplify the solution. The theoretical study is performed by numerically solving the continuity equation of various particle species existing in the discharge cylinder taking into consideration field distortion due to the space charge effect. They hybrid method of characteristics was developed [1] to trace the space and time of the ionization growth under important space charge effect. This method, where continuity equations for electrons and ions are integrated along the characteristics curves, has real advantages and has been used by several authors[2,3,4]. The time interval of this method has been improved[5,6].

As the ionization grows between parallel-plate electrodes, the field distortion takes place due to the space charge of ions and electrons generated by the collisional ionization processes. The one dimensional form of Poisson's equation is used in the computation of space-charge distortion of the electric field[1,5,7,8]. The Poisson's equation assumes that the electric flux passing through the sides of the discharge is negligible compared to that reaching the cathode and anode[1,9]. To overcome this assumption, the disc method is developed to save computing time and to give the axial field distribution to a high degree of accuracy[9,10]. In this method the discharge is divided into discs to calculate the charge at any electric field point. With the appropriate infinite series of discs, the image charge can be obtained by repeated reflections in the electrodes[10-12].

The influence of secondary ionization processes which occur at the cathode is necessary to specify the boundary condition of the equations at the electrode[2,6,13,14]. The photoionization process which results from photons released from deexcitation of excited atoms is one of the secondary mechanisms. The excited atoms or molecules and photons are calculated by continuity equations which involve several excitation levels, excitation coefficient of the levels and the absorption coefficient of photon from the respective level [3,14-16].

In this work, discharge growth between parallel plate electrodes is simulated using various computation techniques. The discharge is followed by solving numerically the continuity equations of electron, positive ion and negative ion using a characteristic method. The electric field is evaluated by the Poisson's equation of one dimension and the disc methods. Secondary electrons due to u.v. light, positive ion and delayed and/or undelayed photon cathode bombardment are included. Photoionization processes are included in the simulation based on solving the continuity equations of excited atoms or molecules and photons. As a subsequence, the framework within this paper selects the most accurate computation technique and applies it to the growth of the discharge to trace the space and time of ionization growth under important space charge effects.

The simulation model is suitable for the two kinds of discharge. The first one is a uniform or a wide discharge, where the radius of the discharge is comparable to the electrode radius. While the second discharge is a filamentary or a narrow discharge, where the radius of the discharge is too small compared to the electrode radius.

2. Continuity Equations

The following basic differential equations[1-3] which relates the particle densities with each other and with other discharge parameters (α, η), and govern the growth of discharge may be derived by considering the rate of gain and loss of charged particles by the elemental volume represented by the lamina of gas of thickness *dx* distance *x* from the cathode, as shown in Fig. 1.

$$\frac{\partial n_e(x,t)}{\partial t} = (\alpha(x,t) - \eta(x,t)) n_e(x,t) w_e(x,t) - \frac{\partial}{\partial x}(n_e(x,t) w_e(x,t)) + Z_p(x,t) \tag{1}$$

$$\frac{\partial n_p(x,t)}{\partial t} = \alpha(x,t) n_e(x,t) w_e(x,t) + \frac{\partial}{\partial x}(n_p(x,t) w_p(x,t)) + Z_p(x,t) \tag{2}$$

$$\frac{\partial n_n(x,t)}{\partial t} = \eta(x,t) n_e(x,t) w_e(x,t) - \frac{\partial}{\partial x}(n_n(x,t) w_n(x,t)) \tag{3}$$

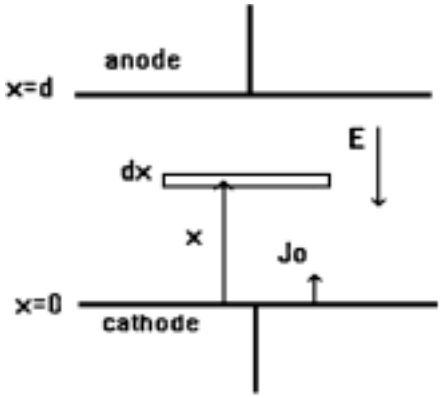

FIG. 1. Discharge gap configuration, J_o is photoelectric density.

where α is the primary ionization coefficient and η is the attachment coefficient. $n_e(x, t)$, $n_p(x, t)$, $n_n(x, t)$ are the electrons, positive ion and the negative ion densities (cm^{-3}) which are functions of distance x and time t. $w_e(x, t)$, $w_p(x, t)$, $w_n(x, t)$ are the corresponding drift velocities (cm/sec), which are functions of distance x and time t. $Z_p(x, t)$ is a term due to photoionization process which is a function of distance x and time t.

The discharge is taken to be of constant radius with uniform particle densities over a cross section, so that only one space dimension needs to be considered in the model. The plus sign appears before the term $\frac{\partial}{\partial x}$ $(n_p(x, t)\ w_p(x, t))$ because the drift velocity $w_p(x, t)$ is always considered positive and the positive ions are moving in the negative x-direction[10].

3. Boundary Conditions

3.1 The Boundary Condition of the Gap Voltage

$$\int_0^d E(x,t)\ dx\ =\ V_g \tag{4}$$

where E is the electric field and V_g(V_g = $V_{applied}$) is the gap voltage which is determined by the characteristic of the external circuit (power supply and the circuit loads). The integral part of equation (4) is evaluated numerically in the simulation at each iteration corresponding to the time t and the computed voltage should be close to the gap voltage V_g. The difference between the computed voltage and the gap voltage V_g represents the error in evaluating electric field.

3.2 The Boundary Condition of the Positive and Negative Ions

$$n_p(d, t) = 0 \tag{5}$$

$$n_n(0, t) = 0 \tag{6}$$

where $n_p(d, t)$, $n_n(0, t)$ are respectively the positive ion density at the anode and the negative ion density at the cathode. In each iteration associated with a specified time t these conditions should be satisfied.

3.3 The Boundary Condition of the Electron at the Cathode

I – Undelayed photon cathode bombardment

If the electrons are produced by the incident undelayed photon (generated photon at time t) on the cathode, such process can be represented by including the following term to the boundary equation of the electron[10]:

$$\gamma_{ph} \int_0^d \alpha(x,t)\ n_e(x,t)\ w_e(x,t)\ dx \tag{7}$$

where γ_{ph} is the probability of the electron emission by undelayed photon cathode bombardment per ionizing collision in the gas.

It can be represented also as[2]:

$$\frac{\Delta x}{w_e(x,t)\ \Delta t} \int_{t_{k-1}}^{t_k} \int_0^d (\frac{\delta_e}{\partial}) \alpha(x,t)\, n_e(x,t)\, w_e(x,t)\ dx\ dt \tag{8}$$

where $\frac{\delta_e}{\alpha}$ is the effective value of the cathode photoemission coefficient measured in spatial growth experiments. Δ_x, Δ_t are respectively the spacing and time intervals in the simulation. In this equation the characteristic method is implemented assuming that the emission of photoelectrons is distributed uniformly. The cathode photoemission is related to the effective value of this factor[2]:

$$\frac{\delta_e}{\alpha} = \frac{\delta}{\alpha} \qquad \text{(Uniform discharge)}, \tag{9}$$

$$\frac{\delta_e}{\alpha} = 10^{-2}\ \frac{\delta}{\alpha} \qquad \text{(Filamentary discharge)} \tag{10}$$

It may be represented also as[1]:

$$\frac{\delta_e}{\alpha} \int_0^d \alpha(x,t)\ n_e(x,t)\ w_e(x,t)\ dx \tag{11}$$

The three above mentioned methods (i.e. equations (7), (8) or (11) are evaluated in the computer program (simulation).

II – Delayed photon cathode bombardment

Assume the photons have a delay time τ_{ph} due to the finite lifetime of the excited states. The effect on accumulated photon up to time t is considered by adding the following term to the electron boundary equation at cathode[10].

$$\frac{\gamma'_{ph}}{\tau_{ph}} \int_0^t e^{(t-t')/\tau_{ph}} \int_0^d \alpha(x,t)\, n_e(x,t)\, w_e(x,t)\ dx\ dt' \tag{12}$$

where γ'_{ph} is the probability of the electron emission due to the accumulated photons by this process per ionizing collision in the gap.

III – Positive ion cathode bombardment

The electrons may be emitted from the cathode by the incidence of a positive ion. This process is included by adding the following term to the electron boundary equation at the cathode[6,10].

$$\gamma_i\, n_p(0, t)\, w_p(0, t) \tag{13}$$

where γ_i is the probability of the electron emission per incident ion. $n_p(0, t)$, $w_p(0, t)$ are respectively the positive ion density and the corresponding drift velocity at the cathode.

IV – Ultraviolet (u.v.) light cathode bombardment

The photoelectric current produced by the external light flash varies with the time according to the relation[6,14]:

$$I_o(t) = I_o(t_o)\, \frac{t}{t_o}\, e^{1-\frac{t}{t_o}} \tag{14}$$

$$J_o(0,t) = \frac{I_o(t)}{A_d} = e\, n_o(t)\ \ w_e(0,t) \tag{15a}$$

where $I_o(t)$, $J_o(t)$, $n_o(t)$, $w_e(0, t)$ are respectively the photoelectric current, the photoelectric current density, the external generated electron density and the corresponding drift velocity at the cathode. A_d , t_o are respectively the discharge area and the time constant of u.v. light. $I_o(t_o)$ is the initial photoelectric current determined by the u.v. light ($I_o(t_o) = 1.163 \times 10^{-9}$ A[6,14]).

The spatial distribution of the avalanche profile at $t = 0$ is evaluated by the following equations[4]:

$$J_o(x,0) = e\, \frac{Z'}{t_o}\, e^{\left(\frac{-x^2}{w^2_{eo} t_o^2} + \alpha_o x\right)} \qquad x \le m t_o\ \ w_{eo} \tag{15b}$$

$$J_o(x,0) = 0 \qquad x > m t_o\ \ w_{eo} \tag{15c}$$

where e is the magnitude of the electron charge and Z' is a constant value chosen so that the total number of the electrons emitted from the cathode under the action of u.v. light is 400 electrons (or any other prescribed value). w_{eo} is the drift velocity of the electron

at $E = E_o$, α_o is Townsend first ionization coefficient at $E = E_o$ and m is a constant value determined by the u.v. light apparatus.

The general equation representing the boundary condition of the electron at the cathode is:

$$J_o(0,t) = e\, n_e(0,t)\, w_e(0,t) = e[n_o(t)\, w_e(0,t) + X1 + \gamma_i n_p(0,t)\;\; w_p(0,t) + \frac{\gamma'_{ph}}{\tau_{ph}} \int_0^t e^{(t-t')/\tau_{ph}} \int_0^d \alpha(x,t)\, n_e(x,t)\, w_e(x,t)\;\; dx\;\; dt'] \tag{16}$$

where $X1$ is the term due to undelayed photon cathode bombardment which could be represented by equation (7) or (8) or (11).

4. Characteristic (Hybrid) Method

As the discharge grows with time, the charged particle densities reach such values that the resultant space charge is no longer negligible, to the extent that the electric field distribution is not constant anymore. Accordingly, various ionization parameters and drift velocities in the continuity equations (1-3) will vary in space and time. The equations are now highly non-linear and have no formal solutions so that it is necessary to model the discharge by using numerical techniques on a digital computer. A number of researchers[2-4,10,15] have developed a successful numerical method known as characteristic or hybrid method based on one space dimension to follow the discharge growth between the two electrodes.

4.1 Simple Continuity Equation

Simple continuity equation can be used by ignoring the photoionization term $Z_p(x, t)$. Thus equation (1) is reformulated as:

$$\frac{dn_e(x,t)}{dt} = \frac{\partial n_e(x,t)}{\partial t} + w_e(x,t)\frac{\partial n_e(x,t)}{\partial x} = (\overline{\alpha}(x,t)\, w_e(x,t) - \frac{\partial w_e(x,t)}{\partial x})\, n_e(x,t) \tag{17}$$

Here $\frac{d}{dt}\,(=\frac{\partial}{\partial t} + w_e\,\frac{\partial}{\partial x})$ represents the derivative evaluated in a frame of reference moving with the electrons, that is along the characteristic curve Δ_c as shown in Fig. 2 and defined by:

$$x - w_e(x, t)\, t = \text{constant} \tag{18}$$

$$\text{or} \qquad dx - w_e(x, t)\, dt = 0 \tag{19}$$

Equation (17) may then be integrated along Δ_c, as follows:

$$n_e(x,t) = n_{eo}(x,t)\, e^{\int_{\Delta c} (\overline{\alpha}(x,t)\, w_e(x,t) - \frac{\partial w_e(x,t)}{\partial x})\; dt} \tag{20}$$

where $n_e(x, t)$, $n_{eo}(x, t)$ are respectively the electron densities at the beginning and at the end of the segment of the curve considered, and $\overline{\alpha}(x, t)$ is the effective ionization coefficient $(\overline{\alpha}(x, t) - \eta(x, t)$.

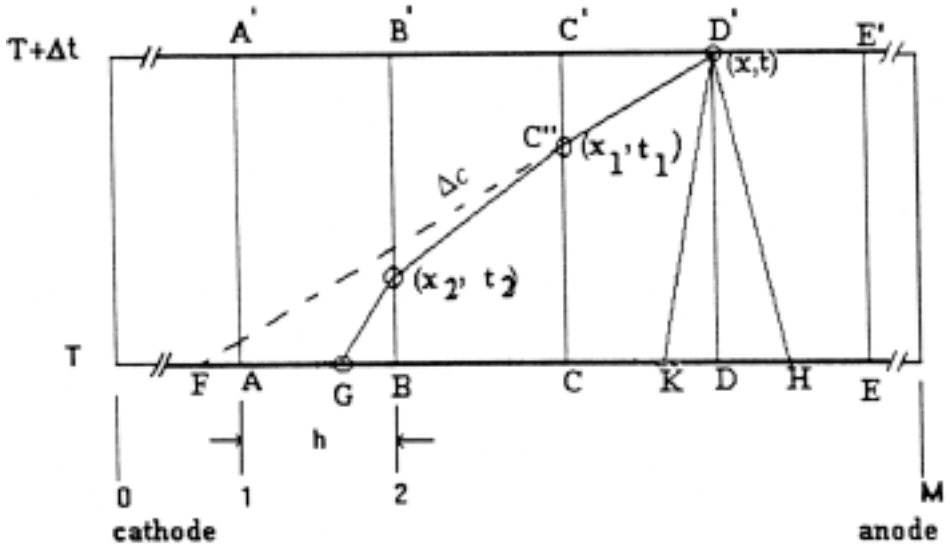

FIG. 2. Characteristic curves traced out by electron and ions reaching point D'.

Suppose the equation (20) has been integrated up to time T and that the tables of all the relevant quantities (n_e, E, ..) have been listed at a set of mesh points as follows:

$$x = 0, h, 2h, 3h, \ldots Mh \equiv \tag{21}$$

where h is the spacing interval value (Δx) in the simulation and M is the number of intervals between electrodes, and it is required to calculate the quantities (n_e , E, ..) at the same mesh points at some later time $T + \Delta_t$. Fig. 2 shows the mesh points at the two instants of time. To calculate $n_e(x, t)$ at the point D', for example, follow the characteristic curves through D' back to the earlier time T. As a first approximation (since none of the variables have been determined at D'), assuming that the field at D' is the same as that at D. It would be possible to trace the characteristic curve back as a straight line to the point F. When it reaches the line CC', a new value for $w_e(C'')$ has to be calculated (equated to w_e at C for the first iteration), to allow for any possible curvature of the characteristic. The coordinate of point C'' is evaluated by equation (19) as follows:

$$\frac{x - x_1}{t - t_1} = w_e(D') \tag{22}$$

The evaluation of t_1 is from equation (22), where w_e (C'') can be evaluated by applying linear interpolation between $w_e(C')$ and $w_e(C)$. This process can be continued to the point G. It becomes necessary to integrate $\bar{\alpha}(x, t)\, w_e(x, t) - \dfrac{\partial w_e(x, t)}{\partial x}$ in the exponent of equation (20) along the characteristic curve Δ_c and interpolate for $n_{eo}(x, t)$ at G. The value of $n_{eo}(x, t)$ at G is found by a 4-point interpolation routine between the neighboring pivotal values (this is being replaced by a 3-point routine at the anode)[5]. The positive

and negative ions are treated similarly as described. However, the incremented movement of the ions is about 1/100th of the distance moved by the electron. There is no need to follow the same curvature of the characteristic, the positive ion's characteristic curve is $D'H$, while the negative ion is $D'K$.

4.2 Manipulation Near Cathode

The electron density at the cathode can affect the electron density at the next few mesh points, as shown in Fig. 3. The characteristic through C', for example can not be continued back to meet the line $t = T$, since it meets the cathode at time greater than T. Equation (20) is therefore modified so that the integral part is evaluated as far as A'', and $n_{eo}(x, t)$ is given the value of $n_e(x, t)$ at A'' by linear interpolation between the values at A and A'. There is therefore a mutual dependence of $n_e(C')$ on $n_e(A')$ and of $n_e(A')$ on $n_e(C')$ due to the excitation taking place at C'. The final result has to be found by iteration. The iterative procedure described above for finding a self-consistent set of $n_e(x, t)$, $n_p(x, t)$, $n_n(x, t)$, $E(x, t)$ will converge to give the correct density $n_e(A')$.

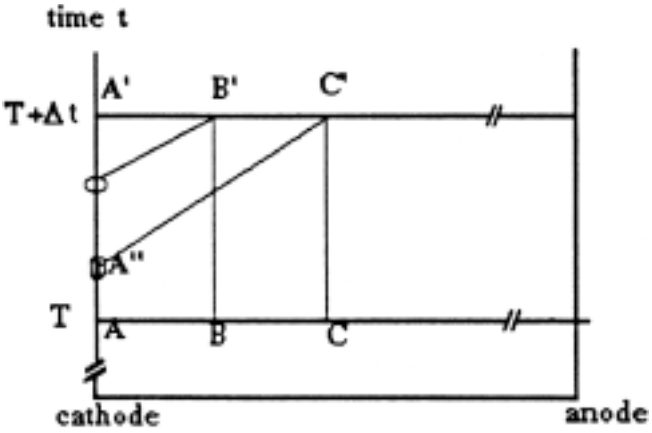

FIG. 3. Characteristic curves manipulation near the cathode.

4.3 Final Step

When $n_e(x, t)$, $n_p(x, t)$, $n_n(x, t)$ have been calculated in the first iteration at all the pivotal points A', B', ... , E', the electric field $E(x, t)$ at time $T + \Delta t$ can be evaluated at the end of first iteration. These procedures are repeated in an iterative manner to obtain more accurate approximations for these quantities. In subsequent iteration, the values of the parameters (*i.e.* $\alpha(x, t)$, $w_e(x, t)$, ...) at a point such as C'' as shown in Fig. 2 are found by linear interpolation between the values at C'' and C which in general are different. The iterative process is repeated until a self-consistent set of results are obtained. The process can then proceed to the next time value.

4.4 Complete form of Continuity Equations

The complete form of continuity equations can be obtained by including the photoionization term $Z_p(x, t)$ and the equations (1-3) can be rewritten as:

$$\frac{dn_e(x,t)}{dt} = \frac{\partial n_e(x,t)}{\partial t} + w_e(x,t)\frac{\partial n_e(x,t)}{\partial x} = P_1(x,t)\, n_e(x,t) + Z_p(x,t) \tag{23}$$

$$\frac{dn_p(x,t)}{dt} = \frac{\partial n_p(x,t)}{\partial t} - w_e(x,t)\frac{\partial n_p(x,t)}{\partial x} = P_2(x,t) + Z_p(x,t) \tag{24}$$

$$\frac{dn_p(x,t)}{dt} = \frac{\partial n_n(x,t)}{\partial t} + w_n(x,t)\frac{\partial n_e(x,t)}{\partial x} = P_3(x,t) \tag{25}$$

$$P_1(x,t) = \overline{\alpha}(x,t) w_e(x,t) - \frac{\partial w_e(x,t)}{\partial x} \tag{26}$$

$$P_2(x,t) = \alpha(x,t) n_e(x,t) w_e(x,t) + n_p(x,t)\frac{\partial w_p(x,t)}{\partial x} \tag{27}$$

$$P_3(x,t) = \eta(x,t) n_e(x,t) w_e(x,t) - n_n(x,t)\frac{\partial w_n(x,t)}{\partial x} \tag{28}$$

The solution of the equations (23-25) are directly evaluated at a certain point (x, t)[3, 17]:

$$n_e(x,t) = e^{\int_{\Delta c} P_1(x,t)\, dt} \left[\int_{\Delta c} Z_p(x,t)\; e^{-\int_{\Delta c} P_1(x',t')\, dt'} dt + n_{eo}(x,t)\right] \tag{29}$$

$$n_p(x,t) = e^{\int_{\Delta c} \frac{\partial w_p(x,t)}{\partial x}\, dt} \left[\int_{\Delta c} (\alpha(x,t)\, w_e(x,t)\, n_e(x,t) + Z_p(x,t)) \right.$$
$$\left. e^{-\int_{\Delta c} \frac{\partial w_p(x',t')}{\partial x}\, dt'} dt + n_{po}(x,t)\right] \tag{30}$$

$$n_n(x,t) = e^{-\int_{\Delta c} \frac{\partial w_n(x,t)}{\partial x}\, dt} \left[\int_{\Delta c} (\eta(x,t)\, w_e(x,t)\, n_e(x,t)) \right.$$
$$\left. e^{\int_{\Delta c} \frac{\partial w_n(x',t)}{\partial x}\, dt'} dt + n_{no}(x,t)\right] \tag{31}$$

The characteristic curve of the electron is represented by equation (19) while for the positive and the negative ions, they are represented respectively as:

$$dx + w_p\, dt = 0 \tag{32}$$

$$dx - w_n\, dt = 0 \tag{33}$$

The integral parts of equations (29-32) are evaluated numerically in the simulation along the characteristic curves of equations (19), (32), and (33).

4.5 Net Particle Species Density Evaluation

If $n_e(x, t)$, $n_p(x, t)$, $n_n(x, t)$ are obtained, the net particle species density $n(x, t)$ can be evaluated as:

$$n(x, t) = n_p(x, t) - n_n(x, t) - n_e(x, t) \tag{34}$$

Using equation (34) leads to a large numerical error in $n(x, t)$ and hence in the resulting electric field $E(x, t)$ which is a function of $n(x, t)$. As stated by Davies *et al.*[6], the stability of the method can be improved by computing the net particle species density by the following equation:

$$\frac{\partial n(x,t)}{\partial t} = \frac{\partial}{\partial x}\left(n_p(x,t)\, w_p(x,t) - n_e(x,t)\, w_e(x,t) - n_n(x,t)\, w_n(x,t)\right) \tag{35}$$

It is therefore preferable in practice to integrate equation (35) to obtain (x, t). The positive ion density $n_p(x, t)$ is evaluated by equation (34) and this significant modification is applied in this work.

4.6 Merits of the Characteristic Method

The numerical solution of a group of hyperbolic partial differential equations has been discussed in a great detail by Morrow[18] who has compared the accuracy and stability of many different algorithms that may be used to solve such equations. He found that the hybrid method of characteristic is an accurate and stable method. This method has a second order accuracy and until recently it was considered as the most commonly used method[10,17]. This method is iterative in nature and could have long execution time even on a high speed computer.

5. Photoionization Process

Photoionization process is included in the simulation and is represented by $Z_p(x, t)$ term. This process is introduced in this work following Yoshida *et al.*[3]. Two more continuity equations are considered; the first one is to represent the metastable atoms or molecules and the second one is to represent photons. Thus

$$\frac{\partial n_m^i(x,t)}{\partial t} = \delta^i(x,t)\, w_e(x,t)\, n_e(x,t) - \frac{n_m^i(x,t)}{\tau_{ph}^i} \tag{36}$$

$$\frac{\partial n_{ph}^i(r,\theta,\phi,t)}{\partial t} = \frac{n_m^i(x,t)}{4\ \pi\ \tau_{ph}^i} - \mu^i C_1 n_{ph}^i(r,\theta,\phi,t) - xC_2 \frac{\partial n_{ph}^i(r,\theta,\phi,t)}{\partial r} \tag{37}$$

where u_m^i , n_{ph}^i are respectively the excited atoms or molecules and the photon densities correspond to the ith excitation level. δ^i, μ^i are respectively the excitation and the absorption coefficients of the ith excitation level. t_{ph}^i , $n_{ph}^i(r, \theta, \phi, t)$ are respectively the lifetime of the excited atom or molecule and the photon density at r in a real space per steradian in the direction of velocity (θ, ϕ) in polar coordinates, C_1, C_2 are respectively the light speed and the photon velocity (C_1, θ, ϕ).

Equation (37) assumes a simple model: once the photon is emitted, it moves on a straight path until it is absorbed. Equation (36) is directly solved at a certain point x, with the initial condition $n_m^i(x, 0) = 0$.

$$n_m^i(x,t) = \int_0^t \delta^i\ w_e(x,t)\, n_e(x,t) e^{-(t-t')} / \tau_{ph}^i\ \ dt' \tag{38}$$

In equation (38) the accumulation of the excited atoms or molecules with the lifetime τ^i_{ph} is considered. This accumulation affects the gas photoionization and the pattern of developed luminosity. Equation (37) is directly solved at a certain point x :

$$n^i_{ph}(x,t) = \frac{1}{4\,\pi\,\tau^i_{ph}\,C_1}\int_0^d \Omega(x')\,e^{-\mu'|x-x'|}\,n^i_m(x, t-\frac{|x-x'|}{C_1}\,dx' \tag{39}$$

where $\Omega(x')$ is the solid angle subtended at x by the cross section of the discharge channel at x'. $|x-x'|$ is the absolute value of the difference between x and x'. The solid angle $\Omega(x')$ is evaluated as[2]:

$$\Omega(x') = 2\,\pi[\,1-\frac{|x'|}{r_p^2+x'^2}\,] \tag{40}$$

where $r_p = 2r$ is for filamentary discharge case and $r_p = r$ is for the uniform discharge case. In a filamentary discharge, it is assumed that all the ions produced by the photoinization process in the region 0-2r are drawn into the developing discharge. The number Z_p of gas photoionization per unit volume is:

$$Z_p(x,t) = C_1 \sum_i \eta'^i\,\mu^i\,n^i_{ph}(x,t) \tag{41}$$

where η'^i is the probability that an absorbed photon will lead to ionization. The summation is taken over all possible excitation levels.

6. Electric Field Computation

6.1 Poisson's Equation Method

The electric field E can be evaluated from Poisson's equation of one dimension[5,8].

$$\frac{\partial\,E(x,t)}{\partial x} = -\frac{-e\;\;n(x,t)}{\varepsilon} \tag{42}$$

where ε is the permittivity ($\varepsilon = \varepsilon_o\,\varepsilon_r$), ε_r is the relative permittivity factor and equals one for all gases, and ε_o is the permittivity of free space and is equal to 8.85×10^{-12} *F/m*[19]. This method is only valid if the radius of the discharge is infinite or of a large value and this is not usually the case in practice[2]. Davies *et al.*[5] have solved numerically Poisson's equation using a relation procedure and the results are compared with the other methods.

6.2 Disc Method

The disc method has been stated by Davies *et al.*[9,10]. In this method a cylinder length d and radius r (discharge channel) is considered as shown in Fig. 4. The distribution of the net electric charge $\rho(x, t)$ ($\rho(x, t) = e\,n\,(x, t)$) considered uniform over any cross section of the cylinder. The field distortion is found at point P on the axis at a distance x from the cathode. The cylinder is divided into a number of discs perpendicular to the axis. The field at P due to a disc of thickness dx' at distance x' from P is

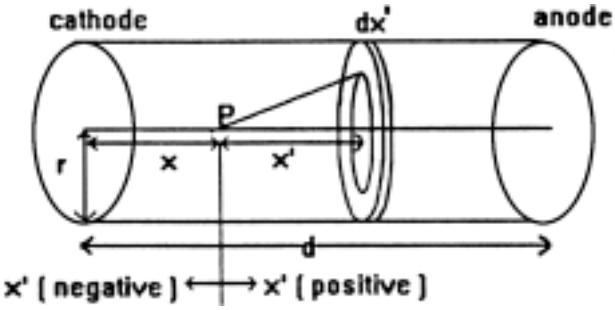

FIG. 4. Basic model to evaluate electric field distortion.

$$\frac{\rho(x+x')}{2\,\varepsilon_0}\left[1-\frac{x'}{\sqrt{x'^2+r^2}}\right]dx' \qquad x'>0 \tag{43}$$

$$\text{and } \frac{-\rho(x+x')}{2\,\varepsilon_o}\left[1+\frac{x'}{\sqrt{x'^2+r^2}}\right]dx' \qquad x'<0 \tag{44}$$

The axial field distortion at P due to all charges in the cylinder is

$$\frac{1}{2\,\varepsilon_o}\left\{\int_{-x}^{0}\rho(x+x')\left[-1-\frac{x'}{\sqrt{x'^2+r^2}}\right]dx'+\int_{0}^{d-x}\left[1-\frac{x'}{\sqrt{x'^2+r^2}}\right]dx'\right\} \tag{45}$$

Since $\rho(x + x')$ is known at all points x, the integral part of the field distortion could be evaluated by a numerical technique either by Simpson or trapzoidal method. In the actual experiment the ends of the cylinder are bound by metal electrodes and thus an infinite series of image charges could be induced in the plates. The effect of these images charges on the field distortion are taken into account by extending the range of integration in equation (45). In general, sufficient accuracy is obtained by considering the images within a distance d on each side of the electrode. The net field intensity on the axis of the discharge is due to two actions, the first is due to an applied field E_o and the second is due to the existing charges in the gap with their images on each side of the electrodes.

$$E(x)=E_o+\frac{1}{2\,\varepsilon_o}\int_{-Lo}^{Lo}\rho(x+x')\left(\frac{x'}{|x'|}-\frac{x'}{\sqrt{x'^2+r^2}}\right)dx' \tag{46}$$

where Lo is taken to include the effect of charge images over the range of d on each side of the electrodes. E_o is the uniform field and is equal to gap voltage over $d(Vg/d)$. The integral part of equation (46) is more accurate whatever is the value of r, compared to Poisson's equation method.

6.3 Basic Theory of Charge Image

The evaluation of the charge image should satisfy the main constraint of both electrodes[11,19] (*i.e.* the induced voltage at both electrodes equals zero due to any point charge and its images).

The point of charge *Qo* at a distance *d-y* from the cathode is shown in Fig. (5). Since the is a scalar quantity, the induced voltage at both electrodes due to charge *Qo* are:

$$V_d = \frac{Qo}{4\,\pi\,\varepsilon_o\,y} \tag{47}$$

$$V_c = \frac{Qo}{4\,\pi\,\varepsilon_o(d-y)} \tag{48}$$

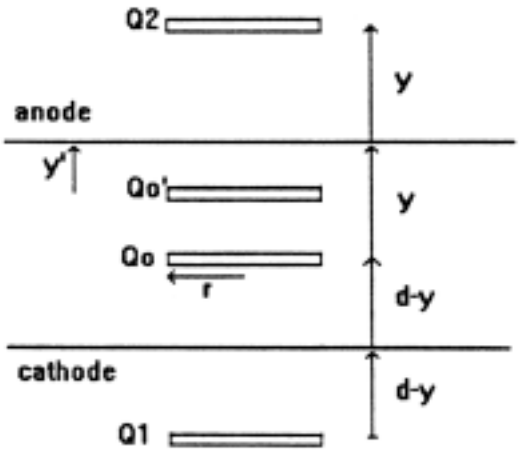

FIG. 5. Basic model to evaluate charge images.

where V_d , V_c are respectively the induced voltage at the anode and the cathode. The charge *Qo* has an image charge inside the cathode represented by *Q*1 at a distance *d-y* from the cathode and inside the anode *Q*2 at a distance *y* from the anode. There are two main conditions to evaluate the charge image. The first one is that the evaluation of any charge images (*e.g. Q*1, *Q*2) is not affected by the other charges in the gap (*e.g. Qo′*) or by their images inside the electrodes (the mutual effect is ignored). The second condition is that the induced voltage at both electrodes due to any charge and its images (*e.g. Q*0, *Q*1, *Q*2) equals zero (the voltage is constant at electrodes).

6.4 Charge Image Evaluation

The induced voltages due to the charge *Qo* and its images *Q*1, *Q*2 as shown in Fig. 5 are represented mathematically as follows:

$$\text{At node } V_d = 0 = \frac{1}{4\,\pi\,\varepsilon_o}\left(\frac{Qo}{y} + \frac{Q2}{y} + \frac{Q1}{2(d-y)+y}\right) \tag{49}$$

$$\text{At cathode } V_c = 0 = \frac{1}{4\,\pi\,\varepsilon_o}\left(\frac{Qo}{(d-y)} + \frac{Q2}{2y+(d-y)} + \frac{Q1}{(d-y)}\right. \tag{50}$$

Equation (49) reduces to:

$$\frac{Qo}{y} = \frac{-Q2}{y} - \frac{Q1}{2(d-y)+y}$$
$$\Rightarrow Q2 = -Qo - \frac{Q1\ y}{2(d-y)+y} \tag{51}$$

Equation (50) reduces to:

$$\frac{Qo}{(d-y)} = \frac{-Q2}{(d-y)+2y} - \frac{Q1}{(d-y)}$$
$$\Rightarrow Q1 = -Qo - \frac{Q2(d-y)}{2y+(d-y)} \tag{52}$$

Substitute equation (52) in equation (51):

$$Q2 = -Qo - \frac{y}{2(d-y)+y}\{-Qo - \frac{Q2(d-y)}{2y+(d-y)}\}$$
$$\Rightarrow Q2 = (-Qo + \frac{Qo\ y}{2(d-y)+y})(1 - \frac{y(d-y)}{(2(d-y)+y)(2y+(d-y))})^{-1} \tag{53}$$

Substitute equation (53) in equation (52) to find $Q1$.

7.1 Total Current and Characteristic Method Accuracy

The total gap current is evaluated as follows[2]:

$$I(t) = \frac{\pi r^2 e}{Eo\ d} \int_0^d n_e(x,t)\, E(x,t)\, w_e(x,t)\, dx \tag{54}$$

The accuracy of the numerical solution of the continuity equations (characteristic method) is checked as follows[4]:

$$\int_0^t [J_e(0,t') - J_e(d,t')]\, dt' - \int_0^d e(n_p(x,t) - n_e(x,t) - n_n(x,t))\, dx = 0 \tag{55}$$

where $J_e(0, t')$, $J_e(d, t')$ are respectively the current densities at the cathode and the anode ($J_e(x, t) = e\ n_e(x, t)\ w_e(x, t)$). As the numerical solution proceeds, the left hand side of the equation (55) differs from zero and when divided by the net charge density $\rho(x, t)$, it yields a measure of the relative error which should not exceed the order of a few percent.

8. Finite Difference Methods (FIDM)

Taylor series expansion about a given nodal point $x = x_i$ is employed to derive the finite difference methods. The following three methods are available in the simulation to evaluate the derivatives equations:

1 – Backward difference method (BDM).
2 – Forward difference method (FDM), whose accuracy is similar to BDM.
3 – Central difference method (CDM), whose accuracy is better than both BDM and FDM.

8.1 Evaluation of the Net Particle Species Density

The net particle density is evaluated by finite difference method using equation (35):

$$\frac{\partial n(x,t)}{\partial t} = \frac{\partial N(x,t)}{\partial x} \tag{56}$$

where $N = n_p(x, t)\, w_p(x, t) - n_e(x, t)\, w_e(x, t) - n_n(x, t)\, w_n(x, t)$. The three finite difference methods are applied on Equation (56) as follow:

$$\frac{n(i,j+1)-n(i,j)}{\Delta t} = \frac{N(i,j)-N(i-1,j)}{\Delta x} \quad \text{(BDM)} \tag{57}$$

$$\frac{n(i,j+1)-n(i,j)}{\Delta t} = \frac{N(i+1,j)-N(i,j)}{\Delta x} \quad \text{(FDM)} \tag{58}$$

$$\frac{n(i,j+1)-n(i,j)}{\Delta t} = \frac{N(i+1,j)-N(i-1,j)}{2\Delta x} \quad \text{(CD} \tag{59}$$

where *i, j* are spacing and time counters as shown in Fig. 6.

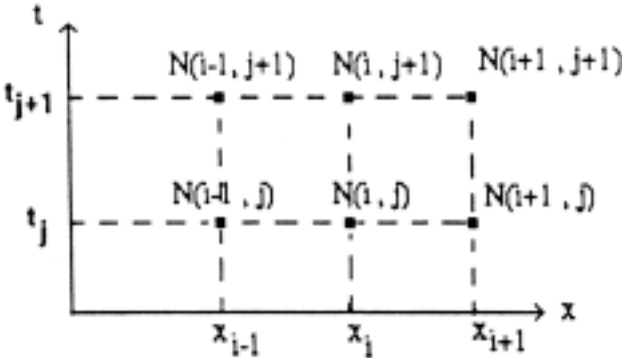

FIG. 6. Derivation of finite difference methods.

8.2 Evaluation of Velocity Partial Derivatives

The derivatives $(\frac{\partial w_e(x,t)}{\partial x}, \frac{\partial w_p(x,t)}{\partial x}, \frac{\partial w_n(x,t)}{\partial x})$ of the velocities may be obtained numerically by using BDM, or FDM, or CDM. This lead to a big error especially near maxima *E* point[5]. The technique has been improved by Davies[6]. As the drift veloci-

ties ($w_e(x, t)$, $w_p(x, t)$, $w_n(x, t)$) where known as functions E, the velocities derivatives had to be deduced analytically as a function of E and $\frac{\partial E}{\partial x}$ [6].

The electric field derivative $\frac{\partial E}{\partial x}$ is given as follows:

$$\frac{\partial E}{\partial x} = \frac{-1}{\varepsilon_1}\{\rho(x) - \frac{r^2}{2}\int_{-Lo}^{Lo} \frac{\rho(x+x')}{(x'^2 + r^2)^{3/2}}\, dx'\} \tag{60}$$

The minus sign appears because the cathode is taken to be $x = 0$ and the anode at $x = d$, whereas conventionally the positive direction of E is from anode to cathode.

The evaluation of net particle density $n(x, t)$ from equation (35), and velocities derivative give a significant modification to the discharge growth modeling. These two modifications enable the growth of a discharge to be traced approximately from 100 to 1000 times further in terms of the final current attained[6].

9. Numerical Integration Techniques

In this simulation two methods are used to evaluate the integrals numerically. The first one is known as trapzoidal method and the second is known as Simpson method.

9.1 Evaluation of Boundary Equation Integration

The boundary equation for electrons at the cathode has an integral term due to the delayed photon equation (12) and is rewritten as:

$$\frac{\gamma'_{ph}}{\tau_{ph}} e^{-t/\tau_{ph}} \int_0^d e^{t'/\tau_{ph}} \int_0^d F_1(x, t')\ dx\ dt \tag{61}$$

$$F_1(x, t') = \alpha(x, t')\, n_e(x, t')\, w_e(x, t') \tag{62}$$

$$F_2(x, t') = e^{t'/\tau_{ph}} \int_0^d F_1(x,\ t')\ dx \tag{63}$$

$$K(t) = \frac{\gamma'_{ph}}{\tau_{ph}} e^{-t/\tau_{ph}} \tag{64}$$

Assume the integration of equation (61) is evaluated up to $t = T$. To evaluate the integration at $t = T + \Delta t$ as shown in Fig. 7, the following equation is used.

$$\int_0^{T+\Delta t} F_2(x, t')\, dt' = \int_0^T F_2(x, t')\, dt' + \Delta t\, \frac{F_2(x, T) + F_2(x, T + \Delta t)}{2} \tag{65}$$

Thus the required integration at $t = T + \Delta t$ is:

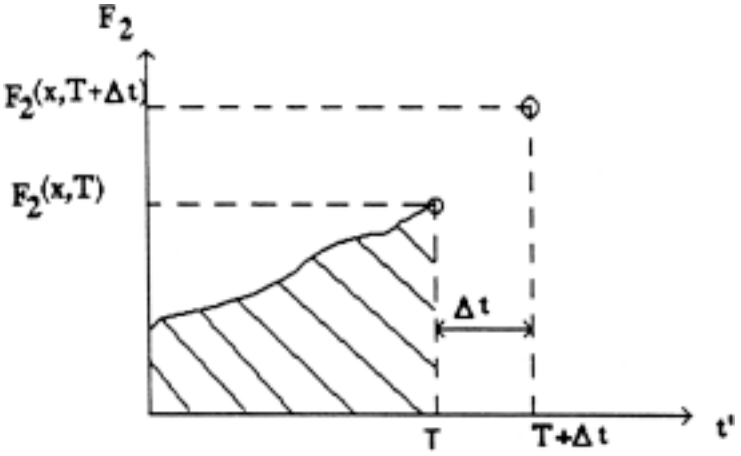

FIG. 7. Illustration of integral evaluation at $T\,\Delta\,Dt$.

$$K(T+\Delta t)\int_{0}^{T+\Delta t} F_2(x,t')\,dt' \tag{66}$$

In the computer program only the values of $\int_{0}^{T} F_2(x,t')\,dt'$ and $f_2(x,t)$ are saved to evaluate the integral part at time $T + \Delta t$.

9.2 Evaluation to Photoionization Process Integration

The integration in equation (39) is evaluated in the simulation by Simpson method, where:

$$0 \le |x-x'| \le d \Rightarrow 0 \le \frac{|x-x'|}{C_1} \le \frac{d}{3}\times 10^{-10} \ \text{sec} \tag{67}$$

The values n^i_m are known numerically at all points while the evaluation of $n^i_m(x', t - \frac{|x-x'|}{C_1}$ may be done by linear interpolation between $n^i_m(x, t - \Delta t)$ and $n^i_m(x, t)$.

10. Simulation Modeling

10.1 Simulation Methods

I – The electric field is evaluated using a disc method by solving equation (46) or one dimensional Poisson's equation method by solving equation (42). The partial derivative $\frac{\partial E}{\partial x}$ of the electric field is evaluated by using the direct formula of equation (60), or by using any finite difference method, *i.e.* FDM using Eq. (57) or BDM using equation (58) or CDM using equation (59). The integration methods of the simulation inte-

grals in equations (4), (46) and (60) may be solved by using Simpson or trapzoidal method.

II – The secondary electron at the cathode due to the cathode particle bombardment is included by using a combination of the right hand side terms of equation (16). This combination should include at least one term other than the u.v. light term (u.v. light effect may be considered or ignored due to the weakness of this factor as the time increases). The photoionization process may be ignored or included. The densities of metastable atoms or molecules and photons are calculated using equations (38) and (39) respectively.

III – The electron density at $T + \Delta t$ by a characteristic method using equation (29) is evaluated. The positive and negative ion densities using equations (30) and (31) respectively are included in the simulation. The net particle species density is evaluated using finite difference method. Thereafter, the positive ion density is recalculated using equation (34). This process is done continuously to predict the required densities values. During this computations the computer program checks the maximum electron density value $n_e\big|_{\text{maximum}}$, if $n_e\big|_{\text{maximum}} > 1 \times 10^8$ cm^{-3} then the electric field is computed by solving equation (46) or (42). The resultant values at all spacing points are taken in a certain time step of 10 *ns*. At a later stage of the discharge near breakdown, the time step in the computer program changes to 1 *ns* to observe the discharge clearly near the breakdown.

10.2 Simulation Conditions

Parallel-plane electrode gap is used with N_2 gas at pressure P = 91 Torr. The discharge parameter such as Townsend first ionization coefficient and drift velocities of different particle species are function of E_o/P = 62 V/cm. Torr. The gap spacing between the two electrodes is d = 3 cm. During simulation the anode voltage is constant and equal to the applied voltage V = 16926 V and the cathode voltage is constant and equal to zero. The required functions and parameters for this simulation are mentioned in Appendix A1.

11. Results and Discussion

11.1 Secondary Process at the Cathode

Figure 8 shows the electron density at the cathode versus time when the delayed and undelayed photon impact at the cathode are considered. Curves 1 and 2 exhibit the undelayed photon impact process with the implementation of equation (8)[10] and 11[1] with $\frac{\delta_e}{\alpha} = 3.1\times10^{-4}$. If the photons have a delay time τ_{ph} due to the lifetime of the excited state, curve 3 shows the effect of the delayed photon cathode impact process. This can be evaluated by equation (12)[14]. As the delayed and undelayed photon cathode impact processes are evaluated with implementation of equation (7) and (12)[14] curve 4 shows higher value of electron density up to 88 nSec than that of curve 2 and the photoionization coefficient γ_{ph} *and* γ'_{ph} are 8.2×10^{-5}.

The effect of positive ion bombardment on the electron density can be clearly seen in Fig. 9 curve 1. This process is evaluated by using equation (13) with $\gamma_i = 10^{-5}$[14].

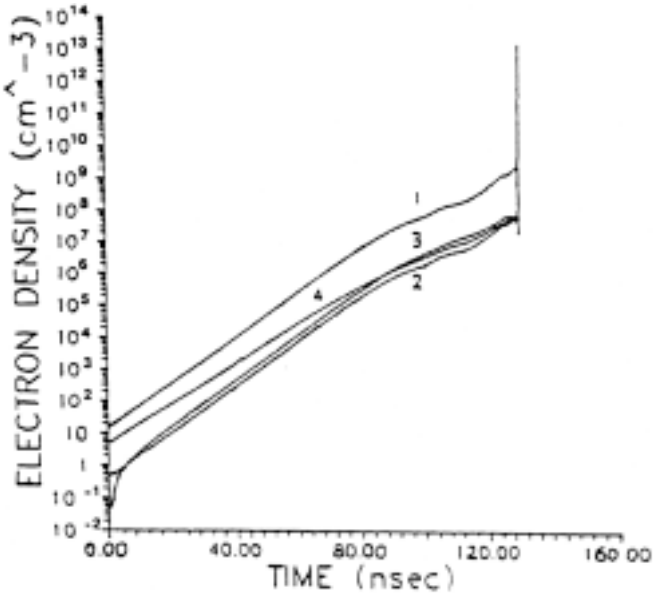

FIG. 8. Electron density at the cathode versus time.
Curve (1) undelayed photon cathode impact process equation (11).
Curve (2) undelayed photon cathode impact process equation (8).
Curve (3) delayed photon cathode impact process equation (12).
Curve (4) delayed and undelayed photon cathode impact process equation (7) and equation (12).

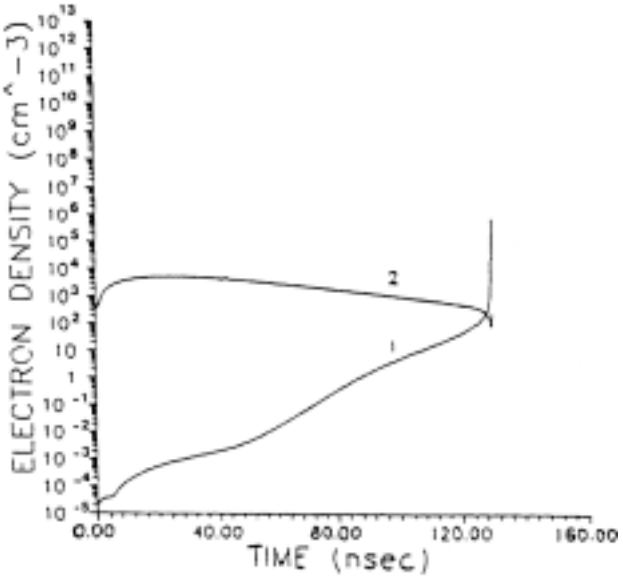

FIG. 9. Electron density at the cathode versus time.
Curve (1) positive ion cathode impact process equation (13).
Curve (2) u.v. light process equation (15a).

The theoretical discharge investigation require applications of u.v. light on the cathode to generate the initial electron pulse which allows the study of the discharge growth clearly. This process is evaluated in the simulation by implementing equation (15a)[8,14]. Figure 9 curve 2 shows the effect of u.v. light on the electron density at the cathode. The secondary electron at the cathode due to an undelayed photon cathode impact process with u.v. light effect are considered in the simulation using equation (16).

11.2 Particle Species Density

Electron density distributions are shown in Fig. 10. The electron density at $t = 0$ has a gaussian distribution which is distorted as the time increases. At $t \geq 30$ ns, the second avalanche maxima near the cathode due to secondary process at the cathode are noticed. The positive ion density is shown in Fig. 11a,b. The electrons and the positive ions acquire energy due to their presence in electric field, which enables the electron avalanche to move towards the anode, and the positive ions to move towards the cathode. Since the primary and secondary electrons are amplified at the same rate, the electron avalanche maxima start to increase so that the secondary electrons approaching the first avalanche find themselves in an enhanced field. The electrons in the second generation have nearly a constant density in the space near the cathode, maintaining the step shown in the electron and the positive ion density curves. The resulting increase in the ionization rate causes the step to move toward the cathode at $t \geq 100$ ns. The first maxima of the avalanche reach the anode at $t \cong 90$ ns. Since the distribution of the electron density controls is the growth of the positive ion density, similarity is noticed between their curves throughout the gap. At $t \geq 105$ ns, the second avalanche maxima disappear due to presenting the secondary electrons in an enhanced field.

11.2.1 Net Particle Species Density Evaluation

The net particle species density is evaluated by solving equation (35) with the implementation of the finite difference methods. Figure 12 shows the net particle species density versus position with the three finite difference method CDM, FDM and BDM. The central difference method (CDM) values exhibit high accuracy near the cathode at a higher time due to the second order accuracy of this method.

11.3 Electric Field Evaluation

The partial $\frac{\partial E}{\partial x}$ of the electric field is evaluated in the program either by direct formula using equation (60) or by any of the finite difference methods. The integration in the direct formula is solved by Simpson or trapzoidal methods which have similar results throughout the gap.

With the implementation of the finite difference methods using Poisson's equation an oscillation is clearly seen throughout the gap due to poor accuracy of this method. Whereas the disc method shows similar value of the electric field partial derivative to that evaluated by Simpson and trapzoidal methods. As the time is increased to $t = 129$ ns the accuracy is reduced near the cathode due to the instability of the numerical techniques. Figure 13 shows the electric field partial derivative using direct formula implementing Simpson method.

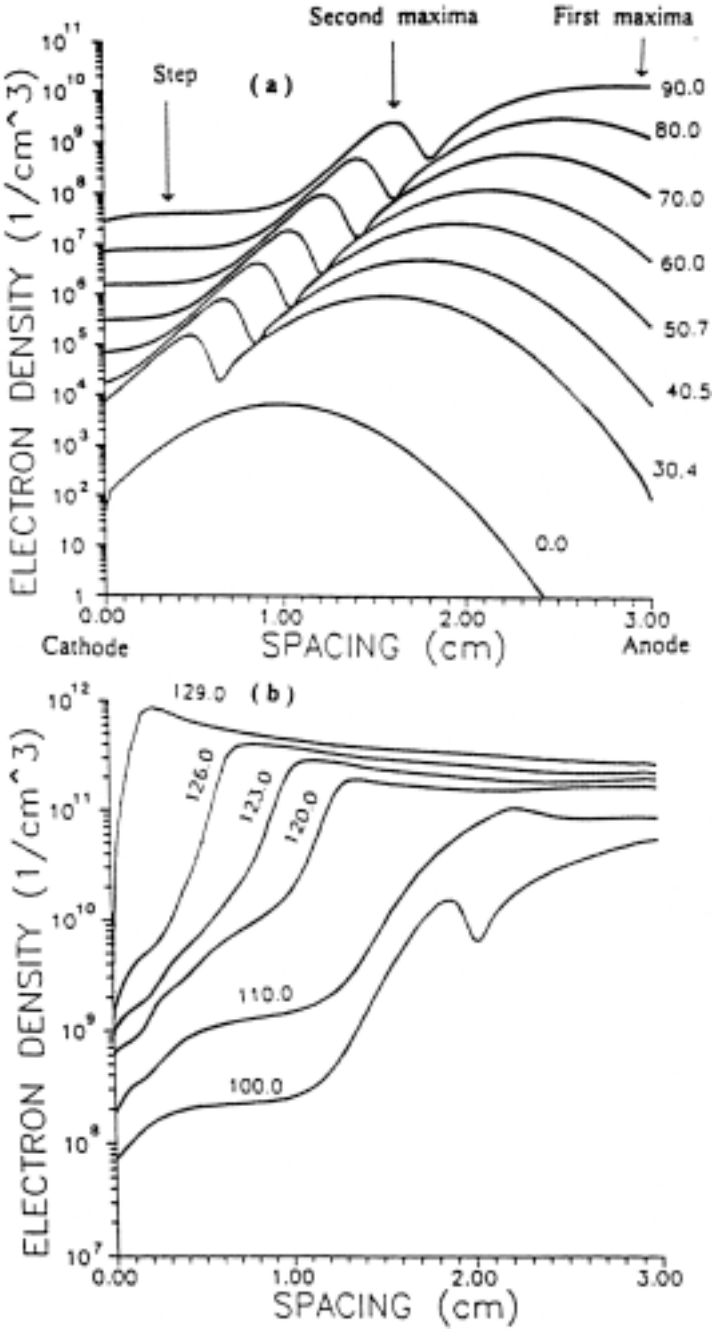

FIG. 10. Numerical computation of electron density versus position. Time in nanoseconds (ns).
(a) 0.0 ns – 90.0 ns.
(b) 100.0 ns – 129 ns.

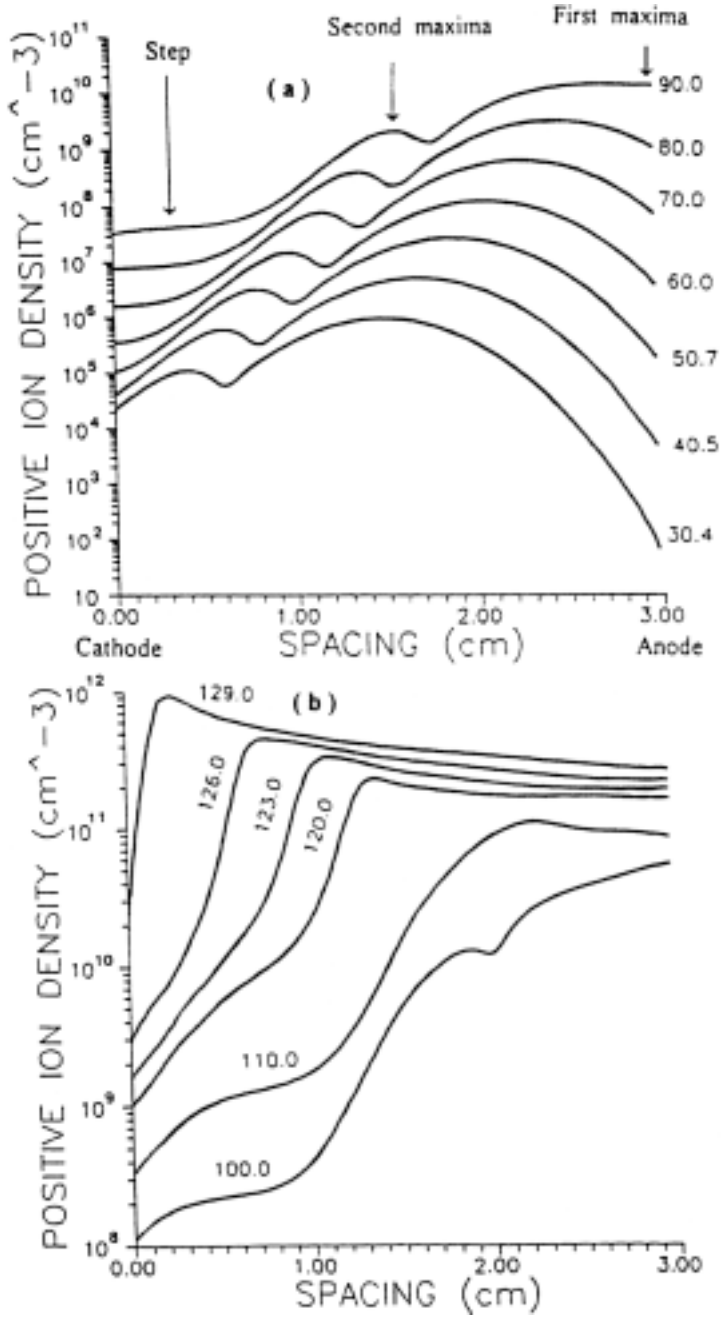

FIG. 11. Numerical computation of positive ion density versus position. Time in nanoseconds (ns).
(a) 0.0 ns – 90.0 ns.
(b) 100.0 ns – 129 ns.

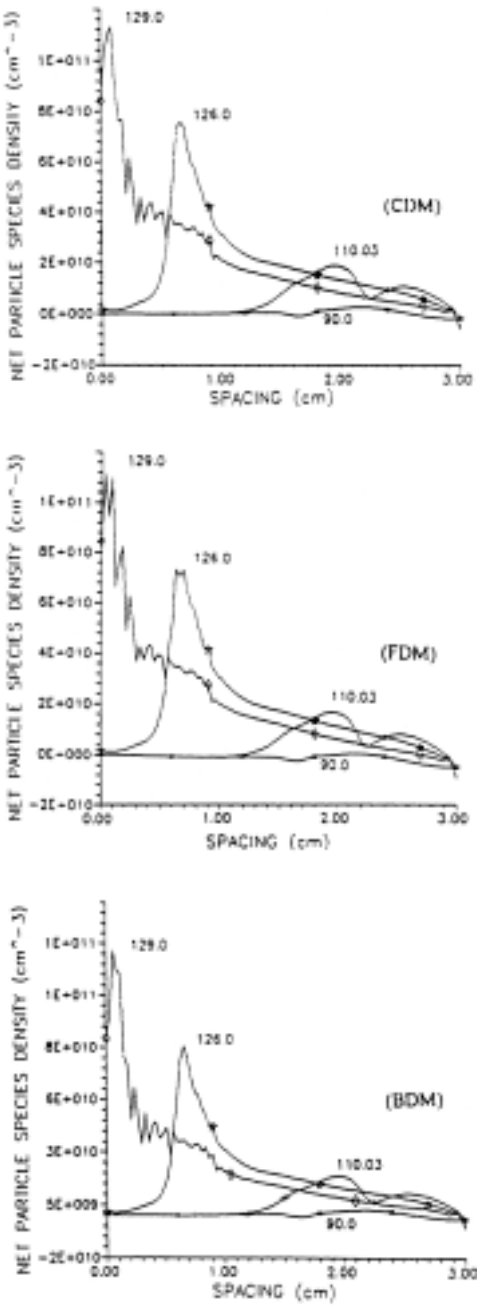

FIG. 12. Net particle species density versus position. Time in nanoseconds.
(a) evaluated by the central difference method (CDM).
(b) evaluated by the forward difference method (FDM).
(c) evaluated by the backward difference method (BDM).

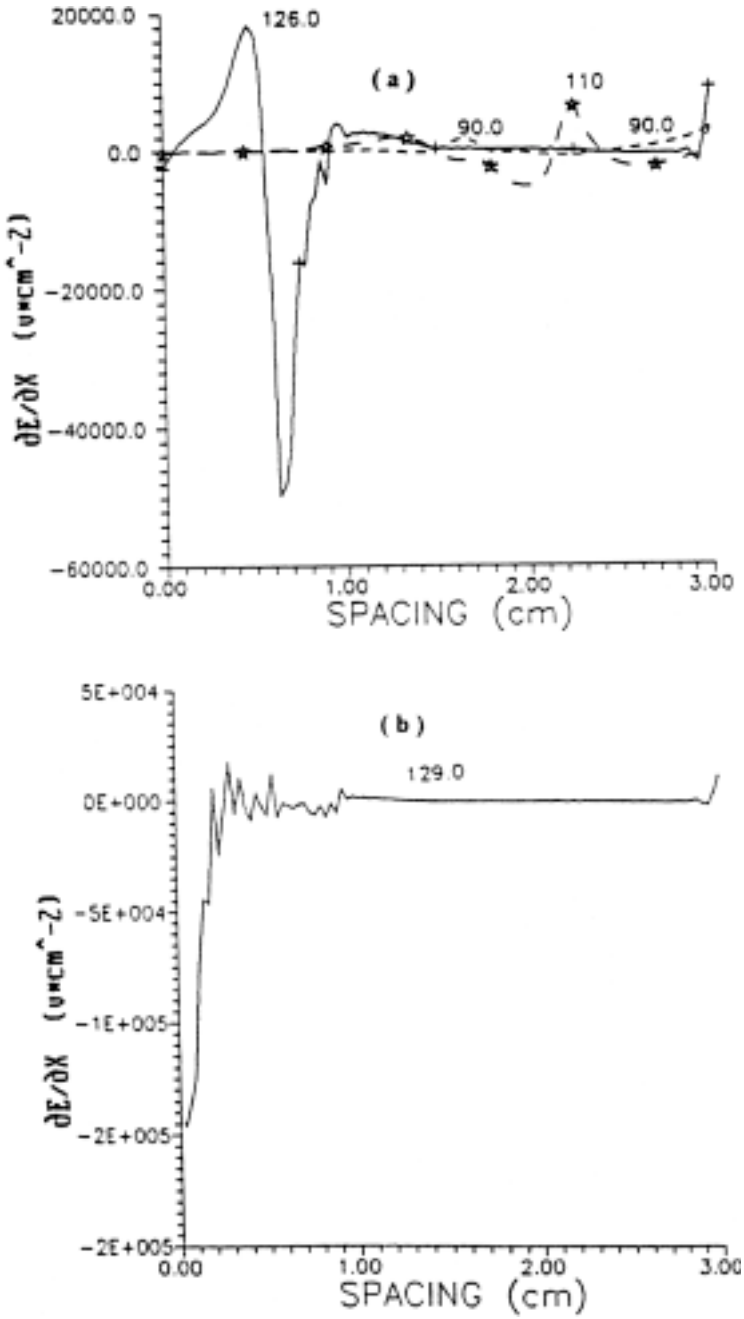

FIG. 13. Electric field derivative versus position. Time in nanoseconds.
(a) 90.0 ns – 126.0 ns.
(b) 129 ns.

In this respect, the electric field is evaluated by using two methods. First by solving one dimensional Poisson's equation as shown in Fig. 14. Second by implementing the disc method as shown in Fig. 15. At t = 90 ns significant difference was noticed at different spacing values. At a later time t = 110 ns the electric field shows higher value with Poisson's equation than that with the disc method due to an increase in the particle species density. The Poisson's equation has poor accuracy in comparison with the disc method and can not follow the quick change of particle species density. The error of Poisson's equation increases with the time as noticed in Table 1.

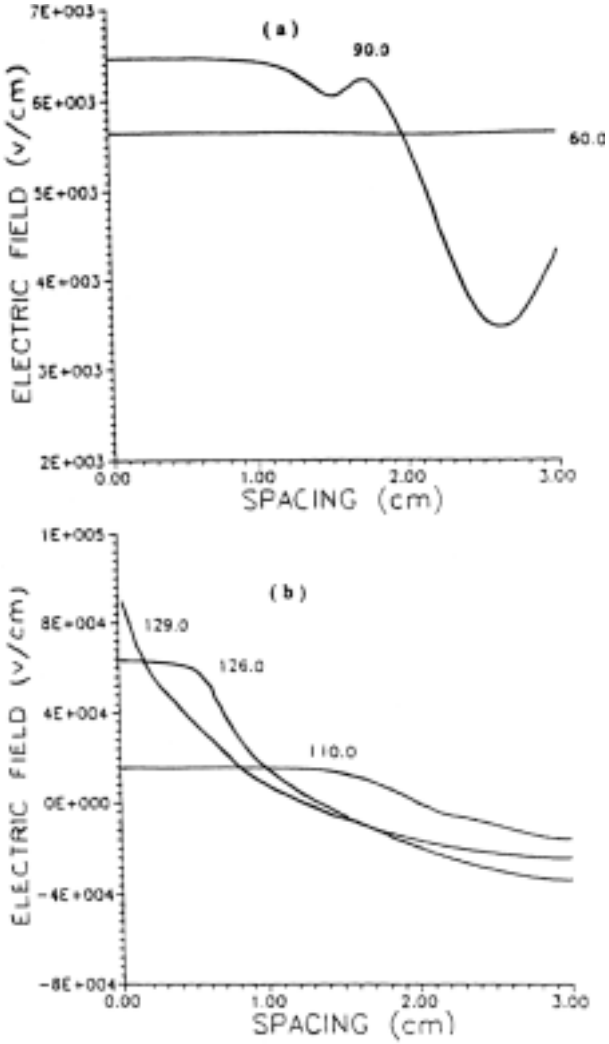

FIG. 14. Electric field distribution versus position using one dimension Poisson's equation. Time in nanoseconds.
(a) 60.0 ns – 90.0 ns.
(b) 110.0 ns – 129.0 ns.

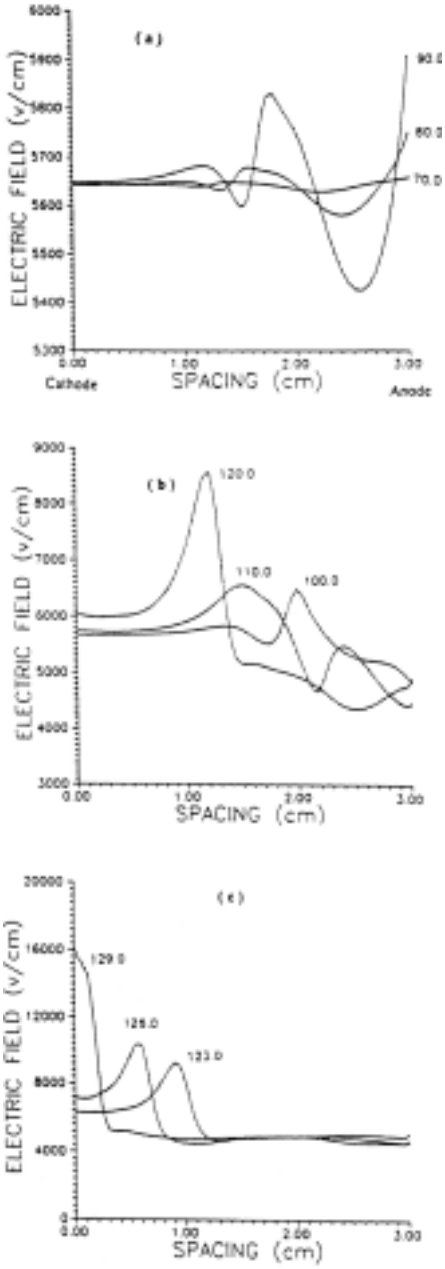

FIG. 15. Electric field distribution versus position using disc method. Time in nanoseconds.
(a) 70.0 ns – 90.0 ns.
(b) 100.0 ns – 120.0 ns.
(c) 123.0 ns – 129.0 ns.

TABLE 1. A comparison of the electric field obtained by the two methods.

Time	Disc method	Poisson's equation	% difference
t = 90 ns	$E(x = 0) \cong 5650$ v/cm $E(x = 1.175) \cong 5830$ v/cm $E(x = 3$ cm$) \cong 5920$ v/cm	$E(x = 0) \cong 6500$ v/cm $E(x = 1.75) \cong 6200$ v/cm $E(x = 3$ cm$) \cong 4300$ v/cm	15 6.3 27.4
t = 110 ns	$E(x = 0)$ 5750 ≅ v/cm $E(x = 1.75) \cong 6600$ v/cm $E(x = 3$ cm$) \cong 4550$ v/cm	$E(x = 0) \cong 16000$ v/cm $E(x = 1.75) \cong 1200$ v/cm $E(x = 3$ cm$) \cong -10000$ v/cm	178.3 81.1 319.8

With the disc method the electric field starts deviation from a uniform field of the value E_o at $t \geq 70$ ns as shown in Fig. 15. At this time a weakly ionised plasma develops and extends with $x \cong 1.5$ cm and $x \cong 2.4$ cm with maximum amplitudes of $n_e(x = 2.34$ cm$) \cong 6.6 \times 10^8$ cm^{-3} $n_p(x = 2.22$ cm$) \cong 6.3 \times 10^8$ cm^{-3} spreading and growing as the time increases. At t = 129 ns, the plasma region is extended through all the gap with maximum amplitudes $n_e(x = 0.28) \cong n_p(x = 0.28) \cong 10^{12}$ cm^{-3}.

11.4 Total Current

Figure 16 shows the evaluated current growth in the gap as a function of time. The second phase starts at t = 100 ns. The breakdown occurs at the time t_b , 130 ns $\geq t_b >$ 129 ns.

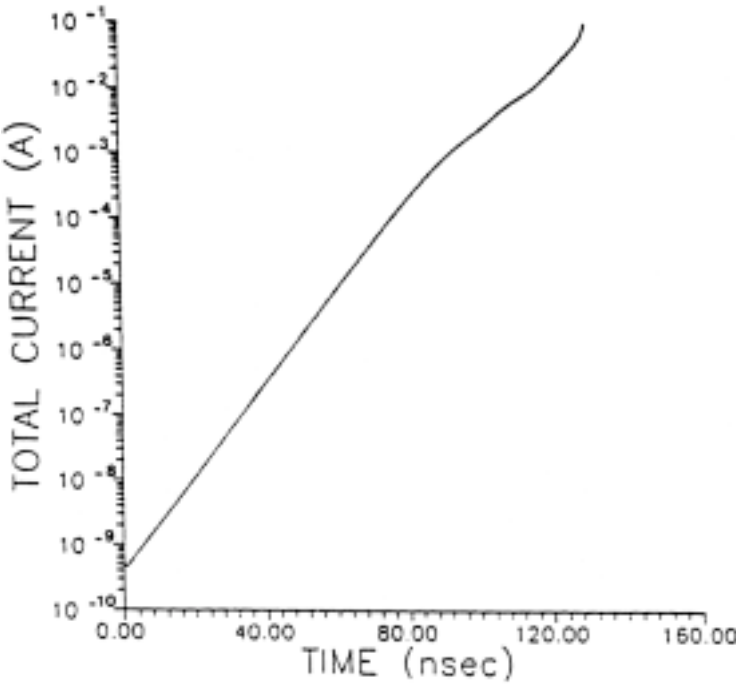

FIG. 16. The growth of the total gap current.

12. Conclusion

The discharge growth in a uniform gap using N_2 gas is investigated by solving numerically the continuity equation of different particle species taking into consideration the field distortion due to the space charge effect. The characteristic method shows high accuracy in solving the continuity equation. The electric field evaluation by disc method presents higher accuracy than that of one dimensional Poisson's equation. The electric field partial derivative $\frac{\partial E}{\partial x}$ using direct formula with Simpson method is used to evaluate the program accuracy. The secondary processes at the cathode tube to u.v. light, positive ion and delayed and/or undelayed photon cathode bombardment are used in the general equation. Further investigation may be carried out to study discharge growth in other dielectric gases in the gap between the electrodes.

References

[1] **Davies, A.J., Evans, C.J.** and **Jones, Llewellyn, F.,** Electrical breakdown of gases: the spatio-temporal growth of ionization in field distorted by space charge; in: *Proc. Roy. Soc.,* **[A] ,** 281: 164-183 (1964).

[2] **Kline, L.E.,** Calculation of discharge initiation in overvolted parallel plane gaps; in: *J. Appl. Phys.,* **45:** 2946-2054 (1974).

[3] **Yoshida, K.** and **Tagashira, H.,** Computer simulation of a nitrogen discharge at high overvoltages; in: *J. Phys. D: Appl. Phys,* **9:** 491-505 (1976).

[4] **Abbas, I.** and **Bayle, P.,** A critical analysis of ionising wave propagation mechanism in breakdown; in: *J. Phys. D: Appl. Phys.,* **13:** 1055-1068 (1980).

[5] **Davies, A.J., Davies, Miss C.S.** and **Evans, C.J.,** Computer simulation of rapidly developing gaseous discharges; in: *IEE Proc.,* **118:** 816-823 (1971).

[6] **Davies, A.J., Evans, C.J.** and **Woodison, P.M.** (1975) Computation of ionization growth at high current densities; in: *IEE Proc.,* **122**(7): 765-768 (1975).

[7] **Reininghaus, Wolf,** Measurement of the space charges produced in streamers; in: *J. Phys. D: Appl. Phys.,* **6:** 982-987 (1973).

[8] **Kulikovsky, A.A.,** The structure of streamers in N_2. I: Fast method of space-charge dominated plasma simulation; in: *J. Phys. D: Appl. Phys.,* **27:** 2556-2563 (1994).

[9] **Davies, A.J.** and **Evans, C.J.,** Field distortion in gaseous discharge between parallel plate electrodes; in: *IEE Proc.,* **114**(10) 1547-1550 (1967).

[10] **Davies, A.J.,** Discharge simulation; in: *IEE Proc.,* **133,** pt. A, No. **4:** 217-240 (1986).

[11] **Yoshida, K.** and **Tagashira, H.,** Computer simulation of a nitrogen discharge considering the radial electron drift; in: *J. Phys. D: Appl. Phys.,* **9:** 485-490 (1976).

[12] **Yoshida, K., Taniguchi, T.** and **Tagashira, H.,** Computer simulation of an axially symmetric narrow discharge at high overvoltage; in: *J. Phys. D: Appl. Phys.,* **12:** L3-L7 (1979).

[13] **Kline, L.E.** and **Siambis, J.G.** (1972) Computer simulation of electrical breakdown in gases; in: *Phys. Rev. A,* **5:** 794-805 (1972).

[14] **Davies, A.J., Evans, C.J., Townsend, P.** and **Woodison, P.M.,** Computation of axial and radial development of discharges between plane parallel electrodes; in: *IEE Proc.,* **124:** 178-182 (1977).

[15] **Bayle, P.** and **Bayle, M.,** Simulation of secondary processes in breakdown in air; in: *Z. Phys. 266,* pp. 275-281 (1974).

[16] **Kulikovsky, A.A.,** Two-dimensional simulation of the positive streamer in N_2 between parallel-plate electrodes; in: *J. Phys. D: Appl. Phys.,* **28:** 2483-2493 (1995).

[17] **Ames, W.F.,** *Numerical Method for Partial Differential Equation.* Academic Press (1977).

[18] **Morrow, R.,** Numerical solution of hyperbolic equation for electron drift in strongly nonuniform electric fields; in: *J. Comp. Phys.,* **43:** 1-15 (1981).

[19] **Kraus** and **Carver,** *Electromagnetics,* Temple Press (1973).

Appendix A1
Nitrogen Simulation Data

A.1.1Functions

$$\frac{\alpha}{P} = 7.56 \; e^{-272P/E} \tag{A1.1}$$

$$w_e = 3.1\times10^5 \;\; E/P \tag{A1.2}$$

$$w_p = \begin{cases} 2\times10^3[1-4\times10^{-3}(E/P)]\;(E/P) & E/P \le 80 \;\; \dfrac{v}{cm \;.\; torr} \\ 1.25\times10^4(E/P)^{1/2} - 2.4(P/E) & E/P > 80 \;\; \dfrac{v}{cm \;.\; torr} \end{cases} \tag{A1.3}$$

$$\frac{\partial w_e}{\partial_x} = \frac{3.1\times10^5}{P}\frac{\partial E}{\partial x} \tag{A1.4}$$

$$\frac{\partial w_p}{\partial x} = \begin{cases} \dfrac{2\times10^3}{P}\dfrac{\partial E}{\partial x}\,[\,1-8\times10^{-3}\;(E/P)\,] & E/P \le 80 \;\; \dfrac{v}{cm \;.\; torr} \\ \dfrac{\partial E}{\partial x}\,[\,\dfrac{1.25\times10^4}{\sqrt{P}}\,\dfrac{1}{2\sqrt{E}} + 2.4\dfrac{P}{E^2}\,] & E/P > 80 \;\; \dfrac{v}{cm \;.\; torr} \end{cases} \tag{A1.5}$$

A1.2 Parameters

The required data are expressed as follows:

1 – The initial number of the electron = 400 electrons, exists between electrodes in a gaussian form[3,5,6,10]. The time constant of u.v. light is t_o = ns[6,14].

2 – The effective value of the cathode photo emission coefficient is $\dfrac{\delta_e}{\alpha}$ 3.1×10^{-4}[5].

3 – The radius of the discharge is r = 0.15 cm[6], r = 2.5 cm[4].

4 – The life time of the excited atom or molecule is τ_{ph} = 14.3 ns[3].

5 – The absorption coefficient of photon μ is assumed to be equal to 10[4]. The probability that an absorbed photon will lead to ionization η' is assumed to be equal to 0.01[4]. The excitation coefficient of the level δ is assumed to be equal to 0.1.

6 – The probability of electron emission by the photon cathode impact γ_{ph} equals to 8.2×10^{-5}[14] .

7 – The time step of the simulation Δt in this work is assumed as:

$$\Delta t = 0.5\,\frac{\Delta x}{w_{eo}} \;\; \text{first phase} \tag{A1.6}$$

$$\begin{aligned} &(n_e\,,n_p)\;|_{\text{maximum}} \;\ge\; 1\times10^8 \qquad \text{then} \qquad \Delta t = 0.5 \;\text{ns} \\ &(n_e\,,n_p)\;|_{\text{maximum}} \;\ge\; 5\times11^{11} \qquad \text{then} \qquad \Delta t = 0.1 \;\text{ns} \end{aligned} \tag{A1.7}$$

where w_{eo} is the electron velocity at $E = E_o$, $(n_e\,,n_p)\,|_{\text{maximum}}$ is the maximum value from n_e and n_p. As the time step Δt is small, the accuracy will be higher, but the program will take more running time.

محاكاة نمو التفريغ الكهربائي بين قطبين متوازيي السطح باستخدام مختلف التقنيات الحسابية

أنور حسن مفتي

قسم الهندسة الكهربائية وهندسة الحاسبات ، كلية الهندسة ، جامعة الملك عبدالعزيز

جـــدة – المملكة العربية السعودية

المستخلص . في هذه الورقة تم بناء محاكاة لنمو التفريغ الكهربائي بين قطبين متوازيي السطح باستخدام مختلف التقنيات الحسابية . لقد استخدمت طريقة التمييز لحل معادلات الاتصال للجسيمات المتنوعة الموجودة في التفريغ الكهربائي . كذلك أمكن إيجاد شدة المجال الكهربائي بطريقة القرص ومعادلة بواسون أحادية البعد . كما تم إدخال الذرات والجزيئات المستثارة والفوتونات نتيجة عملية التأيين الضوئي . كما جري تقييم الإلكترونات الثانوية الناشئة عن قذف المهبط بالضوء فوق البنفسجي والأيونات الموجبة والفوتونات المؤخرة و/ أو غير المؤخرة . في هذا المضمار فإن العديد من هذه التقنيات الحسابية أدت إلي اختيار الطريقة الأكثر دقة في محاكاة التفريغ والتي تساعد علي ملاحقة التفريغ في مراحله المتقدمة . وتم مناقشة التيار الكهربائي الكلي في الثغرة وزمن الانهيار . في هذا البحث تم استخدام غاز النتروجين لدراسة نمو التفريغ الكهربائي .